ELSEVIER

Canadian Association of Radiologists Journal 63 (2012) 18−29

CANADIAN ASSOCIATION OF RADIOLOGISTS JOURNAL

www.carjonline.org

Musculoskeletal Radiology / Radiologie musculo-squelettique

Imaging of Ulnar-Sided Wrist Pain

Rory Porteous, FCRAD Diag (SA)[a], Srinivasan Harish, FRCR, FRCPC[a,b,*], Naveen Parasu, FRCR, FRCPC[a]

[a]*Department of Radiology, McMaster University, Hamilton, Ontario, Canada*
[b]*Department of Diagnostic Imaging, St Joseph's Healthcare Hamilton, Ontario, Canada*

Abstract

Pain on the ulnar side of the wrist is a complex diagnostic dilemma. This is mainly due to the small size and complexity of the anatomical structures. The issue is compounded by the occurrence of positive imaging findings that are clinically asymptomatic. This pictorial essay deals with the imaging manifestations of different causes of ulnar-sided wrist pain.

Résumé

Les cas de douleur du côté cubital du poignet sont difficiles à diagnostiquer, principalement en raison de la petite taille et de la complexité des structures anatomiques. La difficulté s'accentue dans les cas présentant des résultats positifs à l'imagerie sans symptôme clinique. Cet article descriptif traite des manifestations des différentes causes de la douleur du côté cubital du poignet à l'imagerie.

Key Words: Wrist; Imaging; Ulnar-sided pain; MRI

Introduction

Pain on the ulnar side of the wrist is a complex diagnostic dilemma. This is mainly because of the small size and complexity of the anatomical structures in this region. The issue is compounded by the occurrence of positive imaging findings that are clinically asymptomatic. To simplify the problem, sources of ulnar-sided wrist pain can be organized according to the anatomical structures involved. These structures can be considered under the broad categories of cartilage, bone, joint, ligament, tendon, and nerve (Table 1). The various etiologies have been illustrated with images from a 1.5 or 3 Tesla magnet with a 4-channel wrist coil or 16-slice multidetector computed tomography (CT).

Cartilage

Triangular Fibrocartilage Complex

The triangular fibrocartilage complex (TFCC) is generally considered to consist of the triangular fibrocartilage proper (TFC), the dorsal and volar radioulnar ligaments, the ulnar collateral ligament, the meniscal homologue, the sheath of the extensor carpi ulnaris (ECU), and the ulnolunate and ulnotriquetral ligaments [1,2]. On magnetic resonance imaging (MRI), the TFC proper is homogeneously low in signal on all sequences. The ulnar attachment is striated and sometimes has an intermediate signal intensity (Figure 1). The clinical presentation of TFCC injuries usually includes ulnar-sided wrist pain and a palpable or audible click on rotation of the forearm.

Palmer [3] devised a classification system for TFCC tears based on the cause, location, and extent of the abnormality (Table 2), whereby abnormalities are classified as either traumatic (class 1) or degenerative (class 2) (Figures 2−5).

Radiologically, the TFCC may be assessed with conventional MRI, magnetic resonance arthrography (MRA), CT arthrography (CTA), or conventional fluoroscopic

* Address for correspondence: Srinivasan Harish, FRCR, FRCPC, Department of Diagnostic Imaging, St Joseph's Healthcare, 50 Charlton Avenue East, Hamilton, Ontario L8N 4A6, Canada.

E-mail address: sriniharish@gmail.com (S. Harish).

0846-5371/$ - see front matter
doi:10.1016/j.carj.2010.07.007

Table 1
Classification of causes of ulnar-sided wrist pain

Cartilage	Bone	Joint	Ligament	Tendon	Nerve
TFCC pathology	Ulnar styloid fracture	Ulnocarpal impaction	Lunotriquetral ligament tear	Extensor carpi ulnaris tendinopathy and subluxation	Ulnar nerve compression
	Hook of hamate fracture	Ulnar styloid impaction		Flexor carpi ulnaris tendinopathy	
	Kienböck disease	Hamatolunate impaction			
	Ulnar impingement	Pisotriquetral arthropathy			
		Lunotriquetral coalition			
		DRUJ instability			

DRUJ = distal radioulnar joint; TFCC = triangular fibrocartilage complex.

arthrography. The process of selecting a modality involves consideration of a number of factors, such as clinical indication, patient tolerance, radiation exposure, overall cost, and availability.

Triple compartment arthrography has long been used to assess the TFCC, but it lacks specificity in comparison with postarthrography CT and MRI [4]. Moser et al [5], in a comparative study of MRI, CTA, and MRA in 45 cases, demonstrated a slightly superior interobserver agreement, sensitivity, and specificity for TFC tears and cartilage abnormalities by using CTA in comparison with MRA. This is most likely because of the greater spatial resolution of CTA. MRA has a greater contrast resolution and thus has added benefit when assessing the distal attachment of the TFC and bone marrow oedema.

Bone

Ulnocarpal Impaction Secondary to Nonunion of Ulnar Styloid Fracture

Fracture of the ulnar styloid commonly results in nonunion, which may be symptomatic. The un-united fragment may act as a symptomatic loose body. A misaligned fibrous nonunion may impinge on the ECU sheath. Symptoms may arise from an associated avulsion of the ulnar side of the TFC (Palmer class 1B) and associated distal radioulnar joint (DRUJ) instability.

Common MRI findings include visualization of the non-united fragment, triquetral bone marrow oedema, and chondromalacia, with or without subchondral cyst formation (Figure 6).

Hook of Hamate Fracture

The mechanism of injury leading to fracture of the hook of hamate may involve chronic repetitive stress, direct trauma, or avulsion. Complications include ulnar nerve palsy, ulnar artery compromise, and attritional rupture of the fourth and fifth flexor tendons. Investigation of a patient with a typical history and clinical findings should begin with radiographic evaluation. Findings on posteroanterior views include nonvisualization or reduced density of the hamulus. The radially deviated thumb abducted lateral view is more sensitive than the posteroanterior view because it helps to visualize the fracture line. CT or MRI may be used if there is clinical suspicion of a fracture and the plain film findings are questionable (Figure 7).

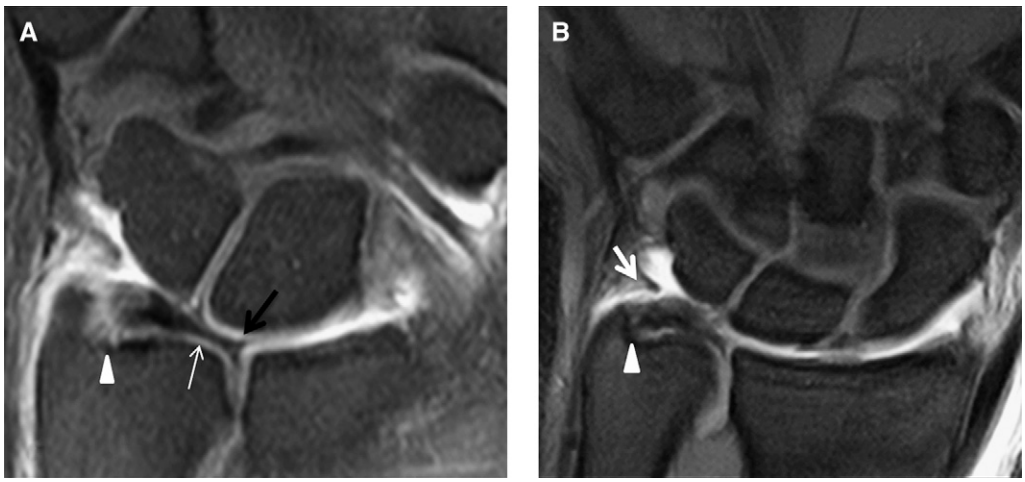

Figure 1. The triangular fibrocartilage complex (TFCC) anatomy. Coronal T1 fat-saturated magnetic resonance arthrogram images (A) and (B), demonstrating the anatomy of the TFCC. Ulnar insertion (arrowheads), the triangular fibrocartilage proper (thin white arrow), radial insertion (thick black arrow) and meniscal homologue (thick white arrow).

Figure 2. Palmer class 1A and 1B lesions. Coronal T1 fat-saturated magnetic resonance arthrographic images, demonstrating Palmer class 1A (A) and class 1B (B) triangular fibrocartilage complex lesions. The images represent different patients. The Palmer class 1A lesion consists of a defect of the triangular fibrocartilage proper (TFC) (thin white arrow) and the Palmer class 1B lesion consists of a tear of the ulnar insertion of the TFC (thick white arrow). Note the presence of gadolinium in the distal radioulnar joint (dotted white arrows).

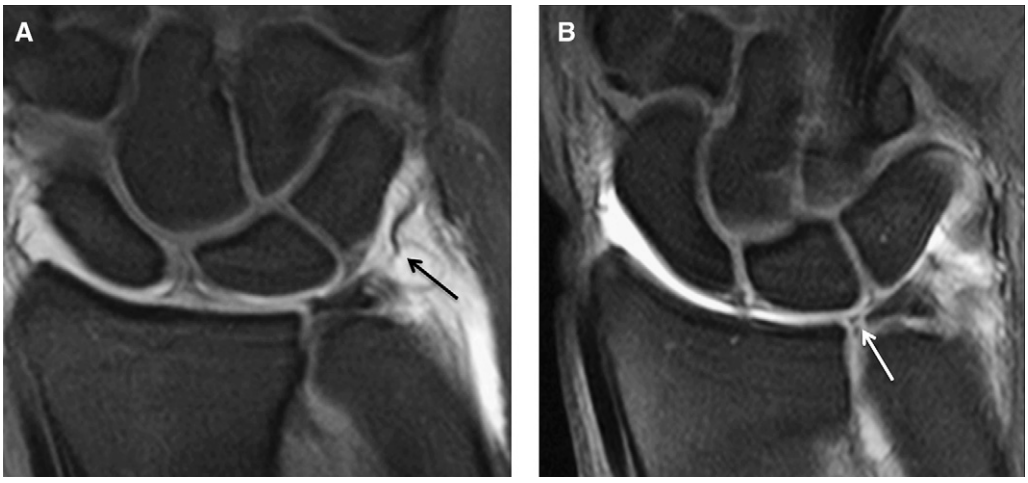

Figure 3. Palmer class 1C and 1D lesions. Coronal T1-weighted fat-saturated MR arthrogram images, demonstrating Palmer class 1 C (A) and class 1D (B) lesions of the triangular fibrocartilage complex (TFCC). The images represent different patients. The class 1C lesion consists of avulsion of the distal attachment of the ulnocarpal and ulnolunate ligaments (black arrow), and the Palmer class 1D lesion consists of avulsion of the radial insertion of the TFCC (white arrow).

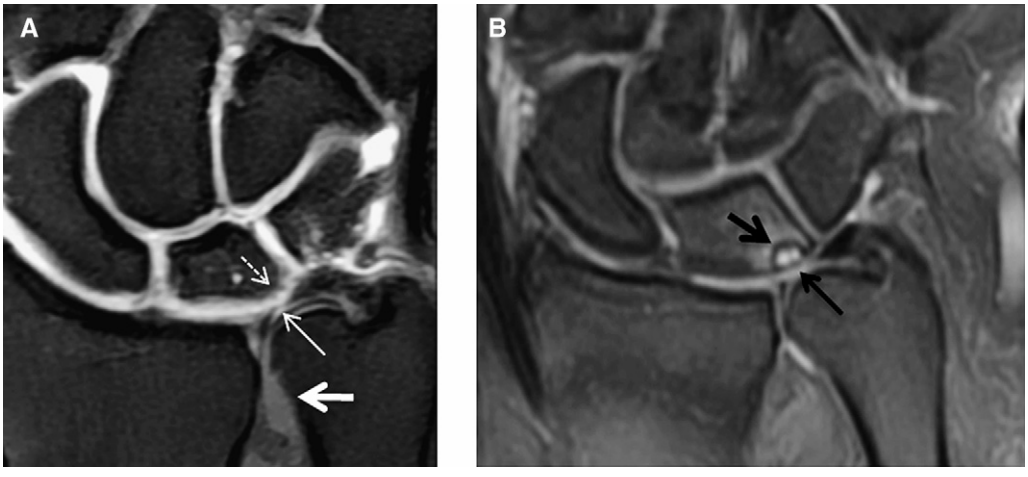

Figure 4. Palmer class 2B and 2C lesions. Coronal T1-weighted fat-saturated magnetic resonance (MR) arthrogram (A) and coronal proton density (PD) fat-saturated (B) MR images, demonstrating Palmer class 2 lesions. The Palmer class 2B lesion (A) consists of triangular fibrocartilage proper (TFC) thinning (thin white arrow) and lunate chondromalacia (dotted white arrow). Note the absence of gadolinium in the distal radioulnar joint (thick white arrow). The class 2C lesion in a different patient (B) consists of TFC perforation (thin black arrow) and lunate chondromalacia. Note the subchondral cyst formation and oedema within the lunate (thick black arrow).

Table 2
Palmer classification of TFCC tears

	Class 1: Traumatic		Class 2: Degenerative
1A:	Central perforation	2A:	TFC wear
1B:	Avulsion of ulnar insertion, with or without an ulna fracture	2B:	TFC wear + lunate and/or ulna chondromalacia
1C:	Distal avulsion	2C:	TFC perforation + lunate and/or ulna chondromalacia
1D:	Radial avulsion, with or without sigmoid notch fracture.	2D:	TFC perforation + lunate and/or ulna chondromalacia + lunotriquetral ligament tear
		2E:	TFC perforation + lunate and/or ulna chondromalacia + lunotriquetral tear + ulnocarpal arthritis

TFC = triangular fibrocartilage proper; TFCC = triangular fibrocartilage complex.

Kienböck Disease

Kienböck disease is a progressive, debilitating process characterized by avascular necrosis of the lunate. It is most commonly associated with negative ulnar variance and is typically unilateral. Predisposing factors are negative ulnar variance and a susceptible lunate geometry (oblong or square).

There are a number of staging systems used. The Lichtman staging classification has the most clinical relevance. There are 4 stages with 2 subcategories in stage 3. In stage 1, the radiographs are normal, with the possible exception of a linear or compression fracture in the lunate. Stage 2 is characterized by a sclerotic lunate, which is either architecturally normal or demonstrates early collapse of the radial side. In stage 3, there is collapse of the entire lunate. The subdivision into 3A and 3B is made by the presence of dynamic rotatory subluxation of the scaphoid in 3A and fixed rotation of the scaphoid combined with proximal migration of the capitate in 3B. Stage 4 is characterized by the presence of generalized arthritic change in the carpus in addition to the findings of stage 3 [6].

MRI in Kienböck disease is useful in staging, and, in particular, it is useful in detecting stage 1 disease because it can demonstrate bone marrow oedema and subtle trabecular microfractures that may be occult on radiography. MRI can also demonstrate the degree of chondromalacia and degenerative change more accurately than radiographs. MRI findings may include bone marrow oedema, reduced T1 and T2 signal intensity as sclerosis develops, and architectural distortion of the lunate progressing from radial-sided to complete collapse (Figure 8).

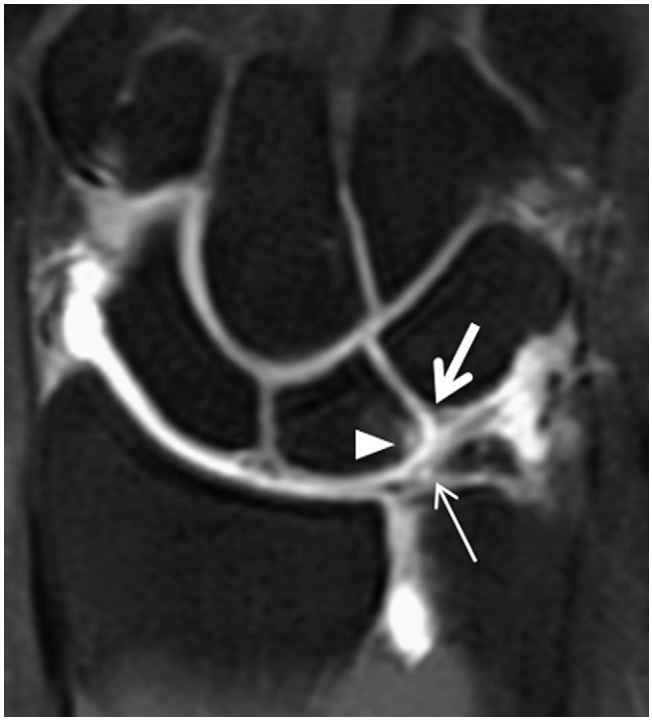

Figure 5. Palmer class 2D lesion. Coronal T1-weighted fat-saturated magnetic resonance image, demonstrating class 2D lesion. The class 2D lesion consists of a triangular fibrocartilage proper perforation (thin white arrow), lunate chondromalacia (white arrowhead), and a lunotriquetral ligament tear (thick white arrow).

Joint

Impaction

Ulnar-sided impaction syndromes are a common source of ulnar pain and limitation of motion that result from repetitive abutment of the distal ulna against the ulnar carpus, distal radius, or surrounding soft tissues, resulting in bone and soft tissue lesions. Impaction is greatly influenced by ulnar variance, which is regarded as the level of the distal ulna relative to that of the lunate notch of the distal radius. Ulnar variance is measured in the neutral position, because supination results in relative ulnar shortening and pronation results in relative ulnar lengthening. Ulnar impaction syndromes are classified into:

1. Ulnocarpal impaction
2. Ulnar styloid impaction
3. Ulnocarpal impaction secondary to nonunion of ulnar styloid
4. Hamolunate impaction
5. Ulnar impingement

Ulnocarpal Impaction Syndrome

Ulnocarpal impaction syndrome is a degenerative condition related to excessive load bearing across the ulnar aspect

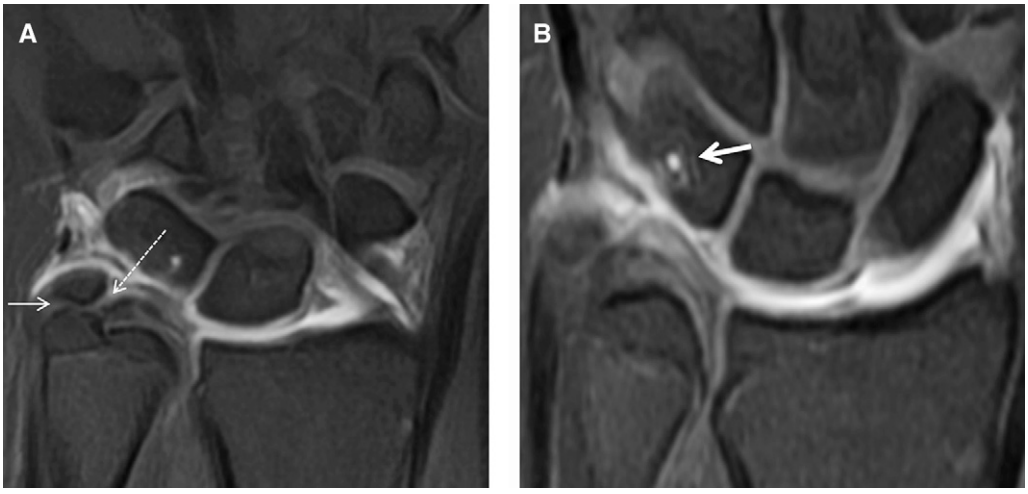

Figure 6. Ulnocarpal impaction because of ulnar styloid nonunion. Coronal T1-weighted fat-saturated magnetic resonance arthrographic images (A) and (B), demonstrating a type 2 ulnar styloid fracture (thin white arrow) and ulnar-sided triangular fibrocartilage proper detachment (dotted white arrow), with evidence of ulnocarpal impaction (thick white arrow).

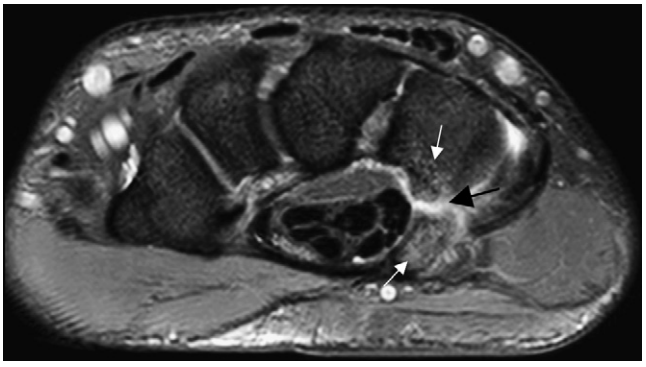

Figure 7. Hook of hamate fracture. Axial proton density weighted fat-saturated image, demonstrating fracture of the hook of hamate (black arrow), with extensive bone marrow oedema in the body and the hook of hamate (white arrows).

of the wrist. Predisposing factors include congenital positive ulnar variance; Madelung deformity; malunited distal radius fractures; radio-ulnar dissociative conditions, such as Galeazzi and Essex-Lopresti fractures; premature closure of the radial growth plate; and excision of the radial head [7].

Pathologic changes seen in ulnocarpal impaction include degenerative (class 2) TFC tear, chondromalacia, luno-triquetral ligament tear, and osteoarthritis of the ulnocarpal and distal radioulnar joints. Radiologic findings (Figure 9) usually include positive ulnar variance. In the early stages, MRI may demonstrate bone marrow oedema and chon-dromalacia in a characteristic distribution in the proximal medial lunate. In established ulnocarpal impaction, there is subchondral sclerosis and cyst formation detectable on radiography [7].

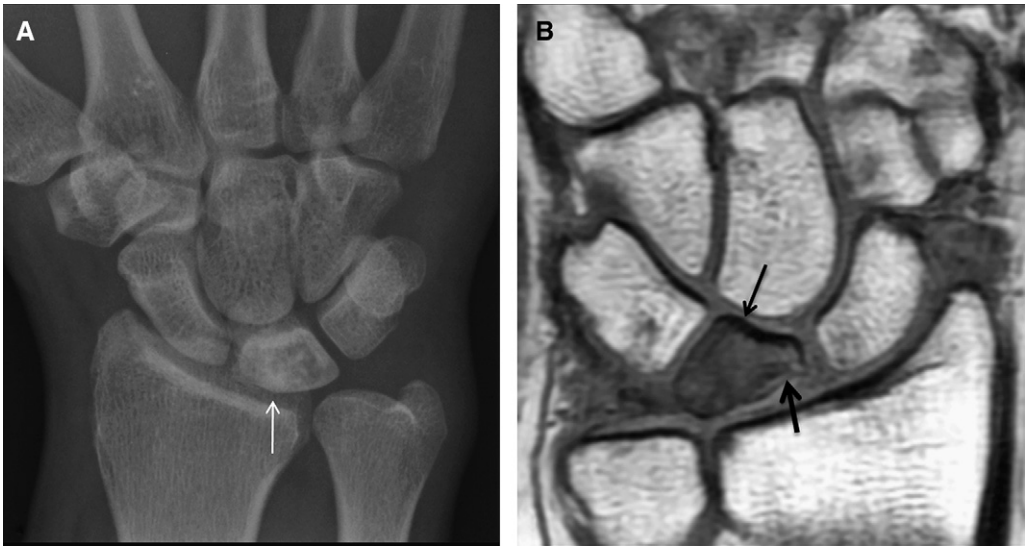

Figure 8. Kienböck disease. Anteroposterior radiograph (A), demonstrating sclerosis of the lunate (white arrow), and, in a different patient, the coronal T1-weighted magnetic resonance image (B), showing diffuse low signal on T1 (thin black arrow) and flattening of the radial aspect of the lunate (thick black arrow).

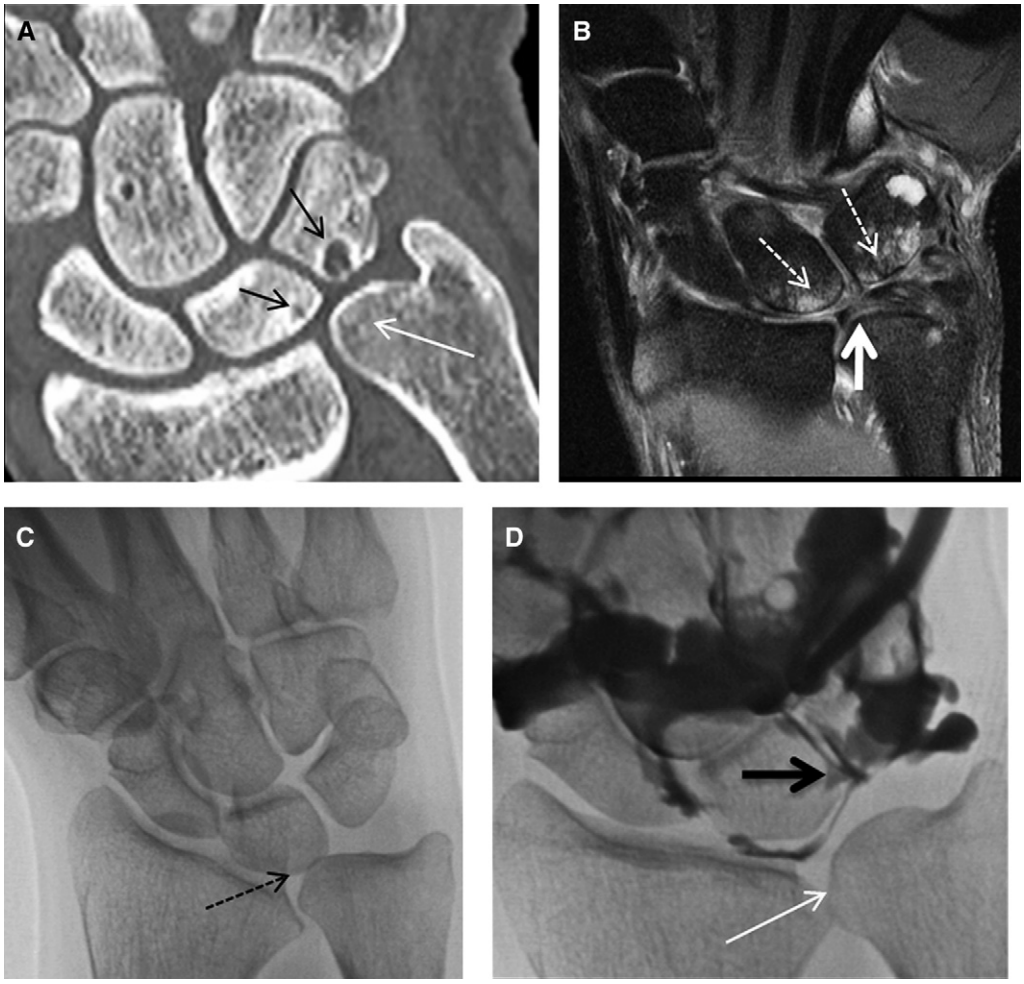

Figure 9. Ulnocarpal impaction. Computed tomographic coronal multi-planar reformat (MPR) (A), coronal proton density fat-saturated magnetic resonance image (B), prone anteroposterior radiograph with clenched fist (C), and fluoroscopic arthrographic image (D), demonstrating ulnar positive variance (thin white arrows), marrow oedema in the lunate and the triquetrum (dotted white arrows), subchondral cyst formation (thin black arrows), a lunotriquetral ligament defect (thick black arrow), and a central triangular fibrocartilage proper defect (thick white arrow). Notice the ulna abutting the lunate in the clenched fist position (dotted black arrow). Images (C) and (D) are of the same patient. Images (A) and (B) are of different patients.

Ulnar Styloid Impaction

This form of impaction is caused by impaction between a long ulnar styloid process and the triquetrum. This is most likely to occur when the wrist is loaded in extension, supination, and ulnar deviation. Repetitive impaction between the ulnar styloid process and the triquetrum results in bone marrow contusion, chondromalacia, and synovitis. Chronic impaction can result in lunotriquetral instability. Radiographic evidence of a long ulnar styloid and a provocative clinical test suggest the diagnosis. MRI can demonstrate a long styloid process, bone marrow oedema, and chondromalacia that involves the ulnar styloid and triquetrum (Figure 10).

Hamatolunate Impaction

The type 1 lunate does not have a facet for articulation with the hamate. Fifty percent of the population has an additional medial facet on the distal lunate, which articulates with the proximal hamate, called type 2 lunate. Ulnar-sided wrist pain is brought on by ulnar deviation of the wrist combined with holding the distal carpal row in supination [8]. In advanced hamatolunate impaction, radiographs will demonstrate arthrosis. MRI findings include bone marrow oedema, chondromalacia, and subchondral cysts in the proximal pole of the hamate or distal/medial lunate (Figure 11). Arthroscopic burring through a mid-carpal portal is the current surgical treatment of choice for this condition [8].

DRUJ

The DRUJ consists of the sigmoid notch of the radius, the head of the ulna, and the TFCC (Figure 12). The dorsal radioulnar ligament tightens in pronation [9]. The stability of the DRUJ is provided by the joint morphology, the capsule, the dorsal and volar radioulnar ligaments, the interosseous membrane, and the myotendinous units of ECU and pronator quadratus [10]. The common abnormalities of the DRUJ are instability, impaction, and incongruity. Incongruity refers to

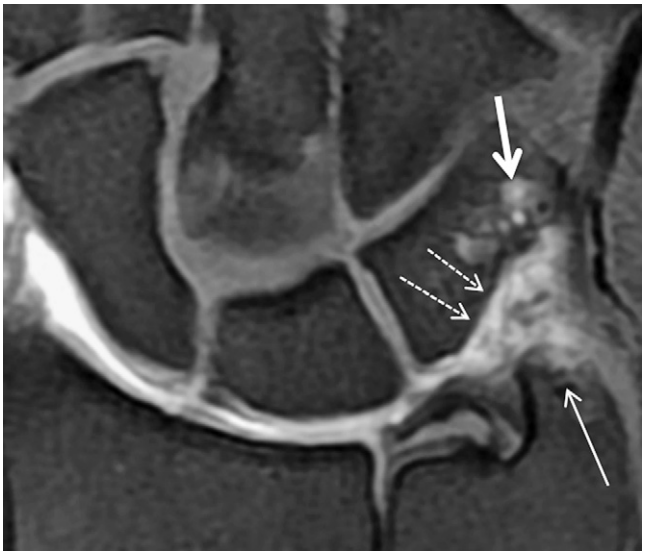

Figure 10. Ulnar styloid impaction. Coronal T1-weighted fat-saturated magnetic resonance arthrographic image, demonstrating a long ulnar styloid process (thin white arrow), triquetral chondromalacia (dotted white arrows), and cyst formation in the triquetrum (thick white arrow).

the lack of a smooth surface between the radius and ulna and can be as a result of osseous trauma or degenerative or inflammatory arthritis.

DRUJ Instability

Instability may be acute or chronic and is usually related to bony abnormalities after a fracture or traumatic soft tissue injury. Instability can result in dorsal or volar subluxation, which may be exacerbated in supination or pronation. There are a number of methods of assessing DRUJ subluxation. All involve acquiring axial images (MRI or CT) in the neutral position, pronation, and supination (Figure 13). Any alteration from this normal geometry indicates subluxation (Figure 14). Investigation with MRI will help confirm instability and detect soft tissue injury (Figure 14) as well as assess secondary chondromalacia and subchondral oedema.

Ulnar Impingement Syndrome

Ulnar impingement syndrome has 3 cardinal features, including a shortened ulna, radio-ulnar convergence, and a pseudarthrosis between the shortened ulna and the ulnar aspect of the distal radius. Radio-ulnar convergence is the approximation of the distal ulna and radius, and occurs as a result of the loss of the buttressing effect of the DRUJ. In long-standing ulnar impingement, an erosive scalloped defect in the cortex of the radius develops. Stress loaded radiographic views and MRI play a role in detecting this condition before the erosive changes occur [11,12]. In the early stages, MRI may demonstrate bone marrow oedema in the opposing portions of the radius and ulna. In the more advanced stages, MRI will demonstrate remodelling of the radius associated with irregularity and sclerosis of the opposing portions of the radius and ulna (Figure 15).

Pisotriquetral Joint

The pisotriquetral joint (PTJ) is a planar synovial joint that communicates with the radiocarpal joint 82%–88% of the time. There are 2 associated synovial lined recesses: the larger is situated superior to the joint and the smaller, inferior to the joint. The most common disorders that affect this joint are arthritis and instability. Patients usually present with chronic pain localized to the hypothenar eminence. Radiographic evaluation of the PTJ is best carried out in the semisupinated oblique view. This allows visualization of the joint space. CT and MRI, with or without arthrography, may be indicated to detect loose bodies and synovial cysts before surgical intervention. Axial and sagittal planes are useful in assessing the PTJ (Figure 16). Cessation of symptoms after a fluoroscopic or ultrasound-guided injection of local anesthetic into the PTJ confirms the pisotriquetral joint as the cause of pain.

Lunotriquetral coalition

Lunotriquetral coalition (LTC) is the most common of all coalitions and has an incidence of 0.1%. DeVilliers Minaar [13] described a classification of LTC, classified into 4 types. Type 1 is characterized by incomplete fusion that resembles a pseudarthrosis, type 2 by partial bony fusion, and type 3 by complete bony fusion. Type 4 includes a type 3 fusion and a co-existent carpal anomaly. LTC may present with chronic pain in the ulnar aspect of the wrist, sometimes related to trauma. Radiographic evaluation of LTC is best carried out on the anteroposterior view. The LT joint space is often

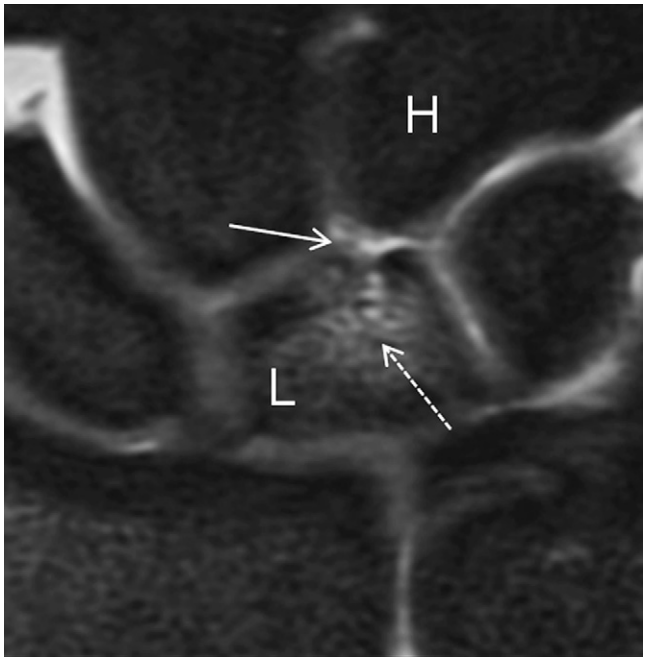

Figure 11. Hamatolunate impaction. Coronal proton density fat-saturated image, demonstrating a type 2 lunate with evidence of hamatolunate impaction. Notice the chondromalacia (white arrow) and bone marrow oedema (dotted white arrow) at the site of impaction. H = hamate; L = lunate.

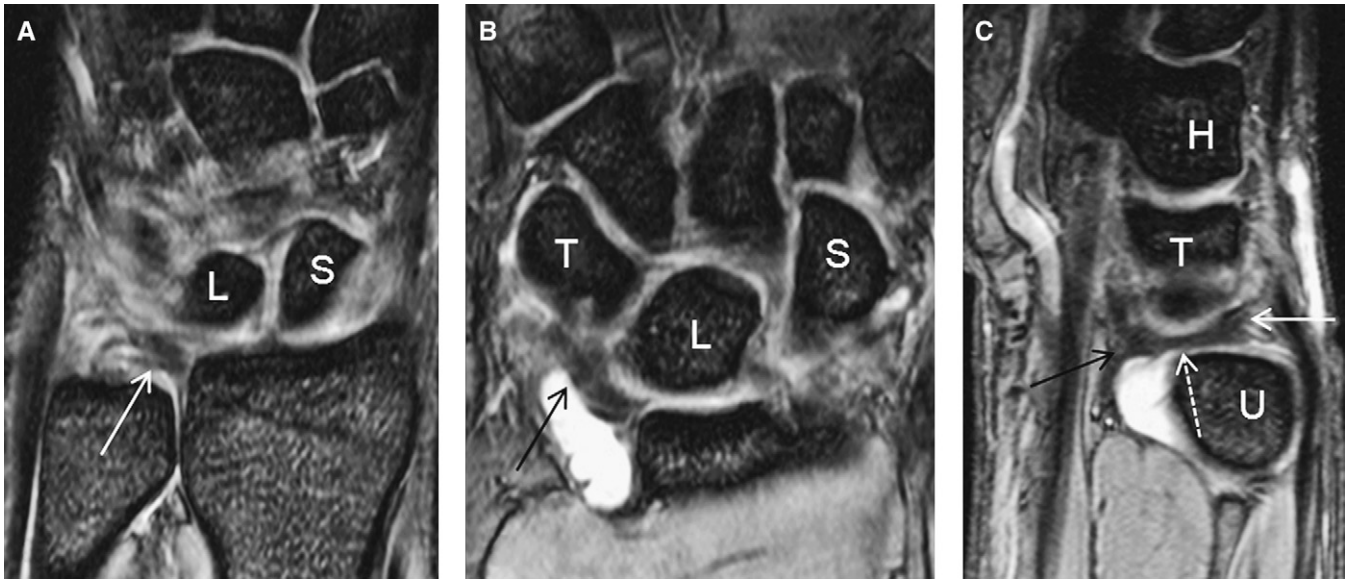

Figure 12. Distal radioulnar joint. Coronal T2-weighted gradient recalled echo (GRE) dorsal (A) and volar (B), sagittal T2-weighted GRE (C), demonstrating the dorsal radioulnar ligament (white arrows), volar radioulnar ligament (black arrows), triangular fibrocartilage proper (dotted white arrow). L = lunate; S = scaphoid; T = triquetrum; H = hamate; U = ulna.

narrowed or absent. CT and MRI can be used to better assess the type of coalition and associated complications. MRI may be useful to exclude the presence of ulnocarpal degenerative change because this may alter the surgical management (Figure 17).

Ligament

Lunotriquetral Ligament

The lunotriquetral ligament (LTL) is composed of 3 distinct regions, with the dorsal and palmar portions being true ligaments and the proximal central portion being a thin membranous structure [14]. The volar portion of the LTL is the greatest contributor to stability in the lunotriquetral region. When there is complete disruption of the ligament between the lunate and the triquetrum, the lunate flexes with the scaphoid and results in volar intercalated segment instability (VISI) [14].

The spectrum of LT injury consists of partial tear, complete tear, and dynamic and static instability. A complete tear may not be sufficient to cause VISI deformity; this requires associated disruption of the radiocarpal ligaments. LTL injuries may be degenerative or traumatic. The degenerative injuries are associated with ulnocarpal impaction and TFC defects.

The LTL may be assessed with conventional MRI, MRA, CTA, or conventional fluoroscopic arthrography. Moser et al [5] demonstrated a superior sensitivity and specificity achieved with CTA when compared with MRA and MRI when assessing partial thickness tears, and a similar sensitivity and specificity achieved with CTA and MRA when assessing complete tears. Nonarthrographic MRI was shown to be inferior to both CTA and MRA. MRI and MRA have far greater

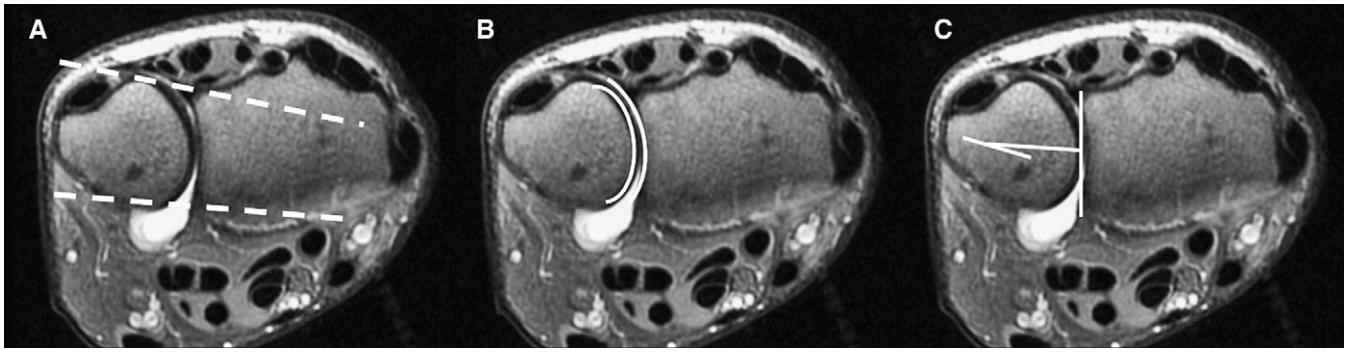

Figure 13. Assessing distal radioulnar joint (DRUJ) alignment. Axial proton density fat-saturated magnetic resonance images, demonstrating the radioulnar line method (A), congruity method (B), and epicentre methods (C) of assessing DRUJ alignment. In the radioulnar line method, the ulnar head is normally situated between 2 lines drawn tangential to the dorsal and volar aspects of the sigmoid notch of the radius. The congruency method demonstrates congruity between the arcs drawn along the articular surfaces of the radius and ulna. The epicentre method involves drawing a line perpendicular to the chord of the sigmoid notch, which normally bisects a line drawn between the centres of the ulnar styloid and the ulnar head.

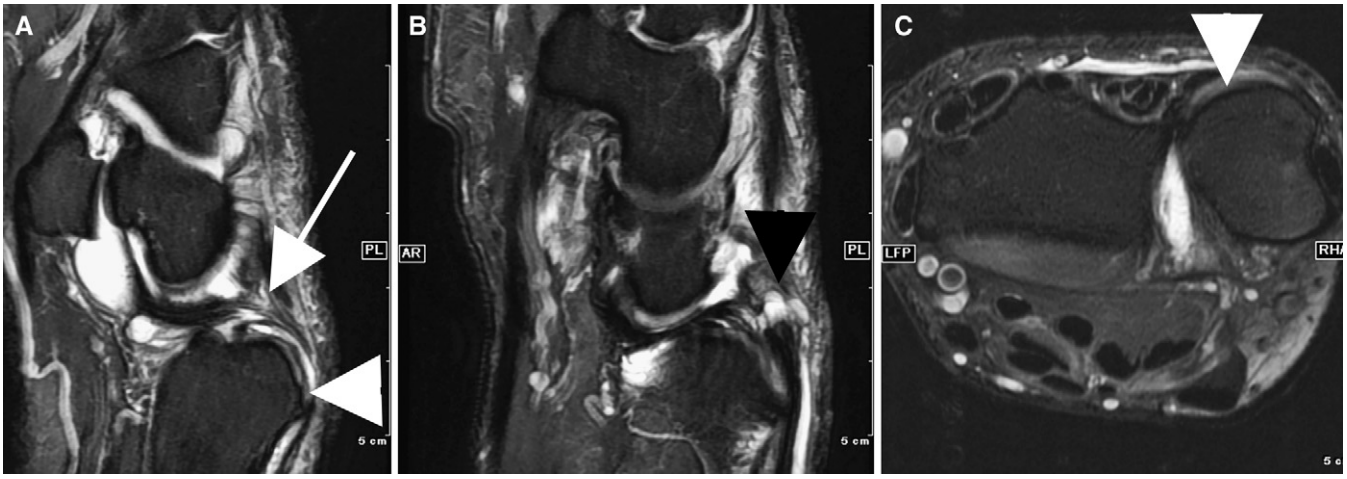

Figure 14. Acute distal radio-ulnar joint subluxation. Sagittal (A, B) and axial (C) proton density–weighted fat-saturated magnetic resonance images, demonstrating dorsal subluxation of the ulnar head (white arrowheads) secondary to surgically proven dorsal radioulnar ligament injury (white arrow), with a ganglion cyst emanating from the ligament (black arrowhead).

contrast resolution and thus offer the benefit of assessing bone marrow oedema and the soft tissues (Figure 18).

Tendon

Extensor Carpi Ulnaris Tendon

The ECU tendon comprises the 6th extensor compartment of the wrist as it passes along the dorsomedial aspect of the distal ulna beneath the dorsal carpal ligament to insert into the ulnar aspect of the base of the 5th metacarpal. The ECU subsheath forms a component of the TFCC and aids in stabilizing the ulnar side of the wrist. The ECU tendon is prone to tenosynovitis and dislocation. Isolated ECU tenosynovitis can occur as a result of an inflammatory process, an acute traumatic event, or repetitive wrist motion (racquet sports). Tenosynovitis is easily diagnosed on either ultrasound or MRI as thickening and fluid distension of the synovial sheath with or without intrasubstance degeneration or tear of the tendon (Figure 19). MRI may demonstrate marrow oedema of the underlying distal ulna.

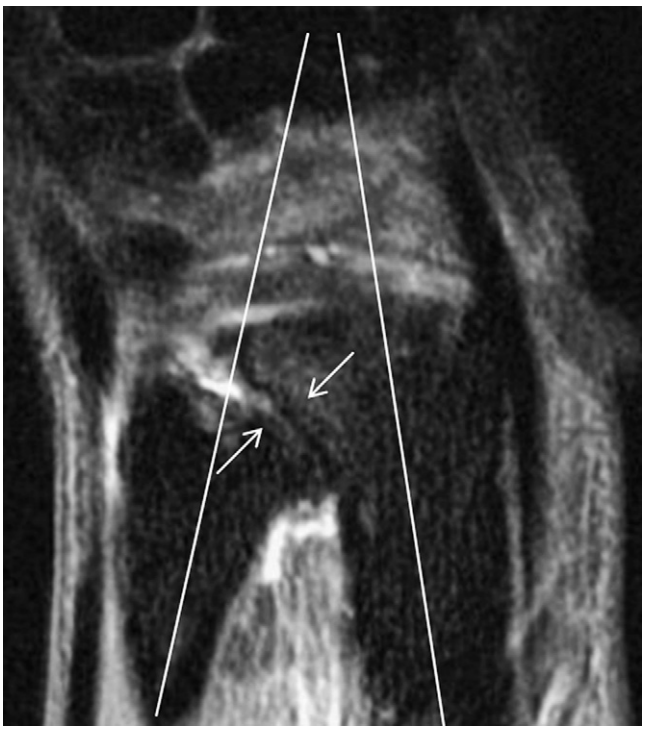

Figure 15. Ulnar impingement syndrome. Coronal short-time inversion recovery magnetic resonance image, demonstrating a short ulna, radioulnar convergence (white lines), and pseudarthrosis between the radius and ulna (white arrows).

Dislocation or subluxation of the ECU tendon occurs as a result of a tear in the ECU subsheath. During supination and ulnar deviation, the ECU dislocates, and, during pronation and radial deviation, the ECU relocates. Sonography has its advantage over MRI in its ability to demonstrate dynamic subluxation (Figure 19).

Flexor Carpi Ulnaris Tendon

The flexor carpi ulnaris (FCU) tendon is situated on the volar aspect of the wrist and inserts into the proximal portion of the pisiform and distally into the hamate and the base of the fifth metacarpal. The spectrum of disease that affects the FCU consists of paratenonitis, tendinosis, and tear. The FCU does not have a tendon sheath. A tear of the FCU can result in PTJ instability.

Nerve

Ulnar Nerve Compression (Guyon Canal Syndrome)

The Guyon canal in the wrist is the second most common site of ulnar nerve entrapment after the elbow. Anatomically, the Guyon canal is composed of 3 zones defined by the level of bifurcation of the ulnar nerve into sensory and motor components [15]. Activities predisposing to ulnar neuropathy

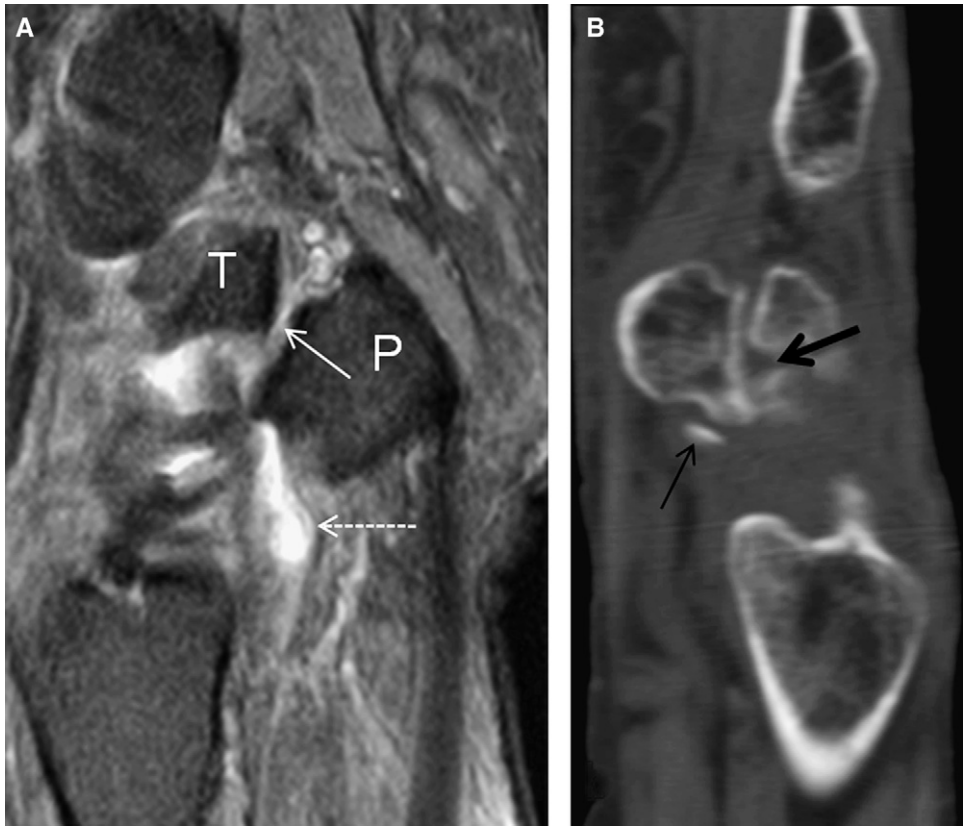

Figure 16. Pisotriquetral joint degenerative change and injury. Sagittal proton density weighted fat-saturated magnetic resonance image (A), demonstrating pisotriquetral joint (PTJ) osteoarthritis. Notice the chondromalacia (white arrow), small joint effusion in the proximal PTJ recess (dotted white arrow). P = pisiform; T = triquetrum. Sagittal reformat CT image (B) in a different patient demonstrating an intra-articular triquetral injury (thick black arrow) with a small bone fragment in the proximal PTJ recess (thin black arrow).

Figure 17. Lunotriquetral coalition. Coronal proton density weighted fat-saturated magnetic resonance arthrogram image, demonstrating an incomplete fibrous coalition (white arrowhead) between the lunate and the triquetrum. Note the narrow joint space and degenerative cyst formation (white arrows) on either side of the coalition.

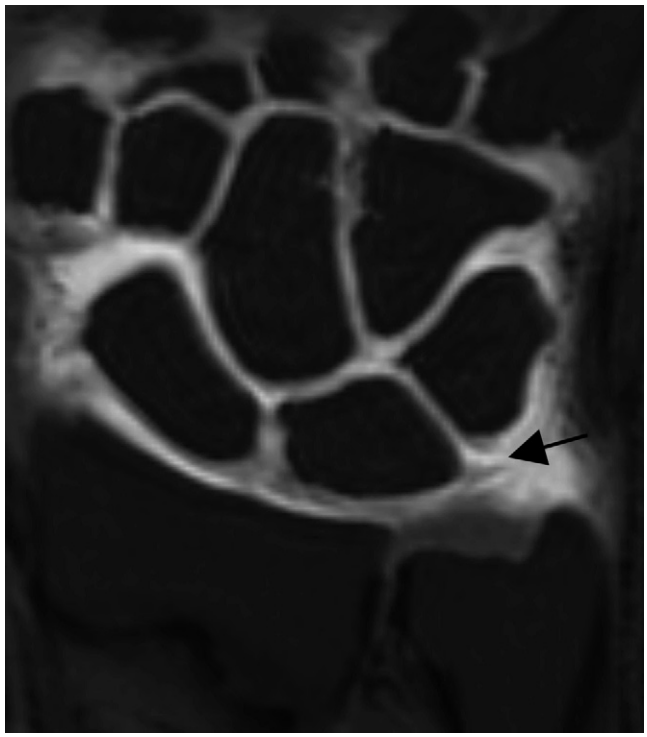

Figure 18. Lunotriquetral ligament tear. Coronal 3D T1-FS gradient echo magnetic resonance arthrogram image, demonstrating a tear of the triquetral attachment of the lunotriquetral ligament (black arrow). Gadolinium injected into the radiocarpal joint has entered the midcarpal space through the tear.

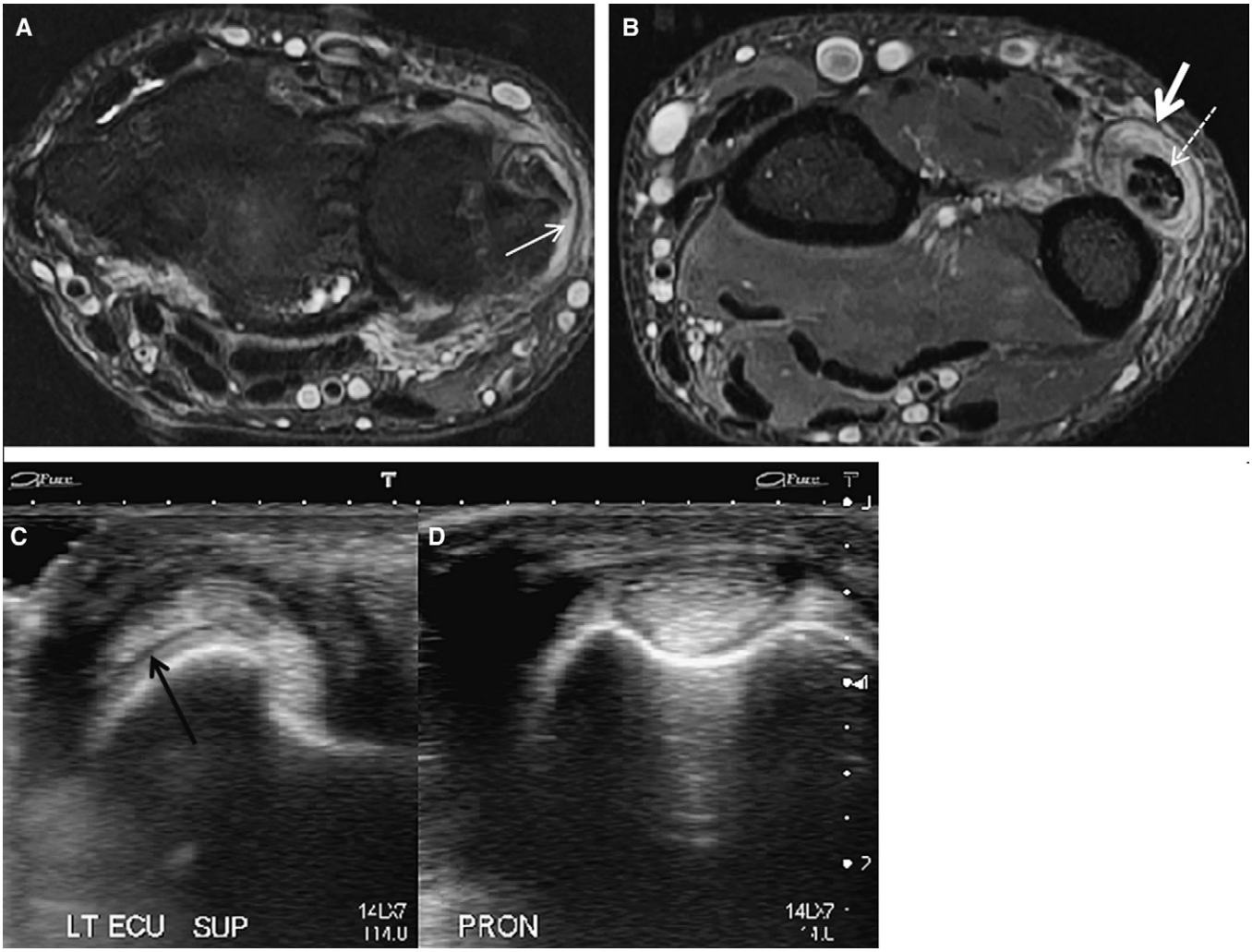

Figure 19. Extensor carpi ulnaris pathology. Axial proton density fat-saturated magnetic resonance images (A) and (B), demonstrating a tear of the volar aspect of the extensor carpi ulnaris (ECU) subsheath (thin white arrow). Notice the longitudinal split tears (dotted white arrow) and tenosynovitis (thick white arrow) that involve the ECU. In a different patient, transverse ultrasound images in supination (C) and pronation (D), demonstrating volar subluxation of the ECU during supination (black arrow).

include vocational activities that result in chronic exposure to vibrations such as the use of pneumatic drills, and activities such as cycling.

Mass effect from adjacent masses such as ganglia, lipoma, accessory muscles, fibrous palmar arch, hook of hamate fracture, os hamuli proprium, ulnar artery aneurysm, and osteoarthritis of the PTJ may all result in ulnar neuropathy.

Clinical manifestations depend on whether the nerve is compressed proximal to the bifurcation, in which case, there will be combined motor and sensory symptoms, or distal to the bifurcation, which could present with either motor or

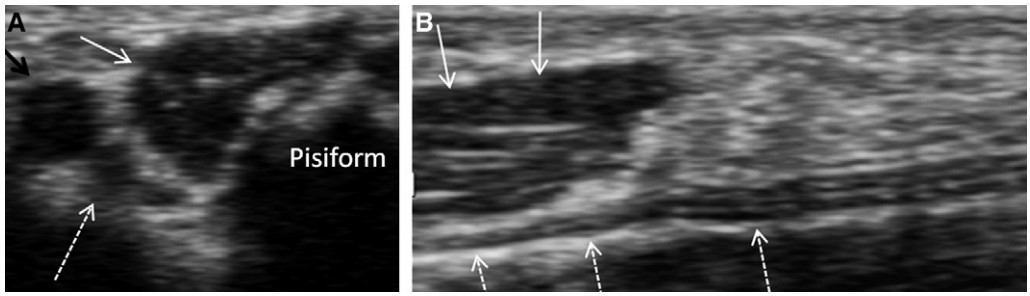

Figure 20. Guyon canal syndrome. Axial (A) and sagittal (B) ultrasound images of the Guyon canal, demonstrating an accessory abductor digiti minimi muscle (white arrows) displacing and compressing the ulnar nerve (dotted white arrows). Ulnar artery (black arrow).

sensory symptoms. If ulnar nerve compromise at the wrist is suspected, then cross-sectional imaging in the form of ultrasound or MRI is useful (Figure 20).

Summary

Ulnar-sided wrist pain can be a diagnostic conundrum for the clinician. Appropriate imaging will aid in making the correct diagnosis, which is essential in the selection of a suitable treatment option. Knowledge of the relevant anatomy, etiology, and clinical features allows a better understanding of the important imaging features that will impact clinical decisions.

References

[1] Zlatkin MB, Rosner J. MR imaging of ligaments and triangular fibrocartilage complex of the wrist. Magn Reson Imaging Clin N Am 2004;12:301–31.
[2] Palmer AK, Werner FW. The triangular fibrocartilage complex of the wrist—anatomy and function. J Hand Surg Am 1981;6:1531–62.
[3] Palmer AK. Triangular fibrocartilage complex lesions. A classification. J Hand Surg Am 1989;14:594.
[4] Levinsohn EM, Rosen ID, Palmer AK. Wrist arthrography: value of the three-compartment injection method. Radiology 1991;179:231–9.
[5] Moser T, Dosch JC, Moussaoui A, et al. Wrist ligament tears: evaluation of MRI and combined MDCT and MR arthrography. AJR Am J Roentgenol 2007;188:1278–86.
[6] Lichtman DM, Alexander AH, Mack GR, et al. Kienbock's disease—update on silicone replacement arthroplasty. J Hand Surg Am 1982;7:343–7.
[7] Friedman SL, Palmer AK. The ulnar impaction syndrome. Hand Clin 1991;7:295–310.
[8] Thurston AJ, Stanley JK. Hamato-lunate impingement: an uncommon cause of ulnar-sided wrist pain. Arthroscopy 2000;16:540–4.
[9] Ward LD, Ambrose CG, Masson MV, et al. The role of the distal radioulnar ligaments, interosseus membrane and joint capsule in distal radioulnar joint stability. J Hand Surg Am 2000;25:341–51.
[10] Gofton WT, Gordon KD, Dunning CE, et al. Soft tissue stabilizers of the distal radioulnar joint: an in vitro kinematic study. J Hand Surg Am 2004;29:423–31.
[11] Lees VC, Scheker LR. The radiological demonstration of dynamic ulnar impingement. J Hand Surg Br 1997;22:448–50.
[12] Cerezal L, del Pinal F, Abascal F, et al. Imaging findings in ulnar-sided wrist impaction syndromes. Radiographics 2002;22:105–21.
[13] DeVilliers Minnaar AB. Congenital fusion of the lunate and triquetral bones in the South African Bantu. J Bone Joint Surg Br 1952;34B:45–8.
[14] Shin AY, Battaglia MJ, Bishop AT. Lunotriquetral instability: diagnosis and treatment. J Am Acad Orthop Surg 2000;8:170–9.
[15] Gross MS, Gelberman RH. The anatomy of the distal ulnar tunnel. Clin Orthop Relat Res 1985;196:238–47.